International Journal of Modern Physics B
Vol. 32 (2018) 1840028 (9 pages)

DOI: 10.1142/S0217979218400283

Effects of noise on fidelity in spin–orbit qubit transformations

L. Ulčakar
J. Stefan Institute, Ljubljana, Slovenia
lara.ulcakar@ijs.si

A. Ramšak*
Faculty of Mathematics and Physics,
University of Ljubljana, Ljubljana, Slovenia
J. Stefan Institute, Ljubljana, Slovenia
anton.ramsak@fmf.uni-lj.si

Accepted 7 February 2018
Published 15 March 2018

We analyze nonadiabatic non-Abelian holonomic transformations of spin-qubits confined to a linear time-dependent harmonic trap with time-dependent Rashba interaction. For this system, exact results can be derived for spin-rotation angle which also enables exact treatment of white gate-noise effects. We concentrate, in particular, on the reliability of cyclic transformations quantified by fidelity defined by the probability that the qubit after one full cycle remains in the ground-state energy manifold. The formalism allows exact analysis of spin transformations that optimize final fidelity. Various examples of time-dependent fidelity probability distributions are presented and discussed.

Keywords: Rashba interaction; holonomic qubit transformation; white noise; fidelity.

PACS numbers: 03.65.Vf, 71.70.Ej, 73.63.Kv, 73.63.Nm, 42.50.Lc

1. Introduction

Spintronics, as a new branch of electronics, is a quantum information technology promising better performance with smaller power consumption.[1–3] The spin of electrons plays the central role[4] and the main challenge is to manipulate the spin of a single electron precisely and locally. Employing magnetic fields, a natural way of spin rotation, usually cannot be applied locally in a small region so other mechanisms should be applied. A possible such solution is to use semiconductor heterostructures[5,6] with spin–orbit interaction (SOI) and particularly strong Rashba interaction[7,8] that can be tuned externally using voltage gates.[9–19]

*Corresponding author.

Recently, a simple scheme for the spin-qubit manipulation was proposed in which an electron is driven along a linear quantum wire with time-dependent SOI, tuned by external time-dependent potential.[20,21] One limitation of such linear systems is posed by fixed axis of spin rotation, but it can be eliminated in quantum ring structures, exhibiting a rich range of phenomena.[22–29] For quantum ring structures consisting of a narrow ring with superimposed time-dependent harmonic trap and controllable time-dependent Rashba interaction, the exact solutions were presented most recently.[30,31]

In linear as well as in ring systems controlled by external gates there are several possible sources of noise which cannot be avoided. In particular, noise can be induced due to fluctuating electric fields, caused by the piezoelectric phonons[32–35] or due to phonon-mediated instabilities in molecular systems with phonon-assisted potential barriers, which introduce noise in the confining potentials.[36,37] For qubits realized as spin of electrons carried by surface acoustic waves the noise can be caused by the electron–electron interaction.[38–40] Since exact solutions for qubit manipulation scheme considered here are possible, the analysis of environment effects can for some sources of noise be performed analytically.[41]

The paper is organized as follows. After the introduction, Sec. 2 presents the model where also a brief overview of the exact solution together with the analysis of effects due to white noise is revealed. Section 3 is devoted to the fidelity of qubit transformations. The derivation of influences of noise on fidelity is presented in detail and explicit examples are given. Results are summarized in Sec. 4.

2. Model, Exact Solution and White Noise

We consider an electron in a quantum wire confined in a harmonic trap.[20,21] The center of such one-dimensional quantum dot, $\xi(t)$, can be arbitrarily translated along the wire by means of time-dependent external electric fields. Spin–orbit Rashba interaction couples the electron spin with orbital motion, resulting in the Hamiltonian

$$H(t) = \frac{p^2}{2m^*} I + \frac{m^*\omega^2}{2}[x - \xi(t)]^2 I + \alpha(t) p\, \mathbf{n}\cdot\boldsymbol{\sigma}, \tag{1}$$

where m^* is the electron effective mass, ω is the frequency of the harmonic trap, $\alpha(t)$ is the strength of SOI, possibly time-dependent due to appropriate time-dependent external electric fields. The spin-rotation axis $\mathbf{n}$ is fixed and depends on the crystal structure of the quasi-one-dimensional material used and the direction of the applied electric field.[44] $\boldsymbol{\sigma}$ and I are Pauli spin matrices and unity operator in spin space, respectively, and p is the momentum operator. Exact solution of the time-dependent Schrödinger equation corresponding to the Hamiltonian equation (1) is given by[21]

$$|\Psi_{ms}(t)\rangle = e^{-i[\theta(t) I + \phi(t)\mathbf{n}\cdot\boldsymbol{\sigma}/2)]} \mathcal{A}_\alpha \mathcal{X}_\xi |\psi_m(x)\rangle |\chi_s\rangle, \tag{2}$$

$$\theta(t) = \omega_m t + \phi_\alpha(t) + \phi_\xi(t) + m^* \dot{a}_c(t) a_c(t)/\omega^2, \tag{3}$$

$$\mathcal{A}_\alpha = e^{-i\dot{a}_c(t) p \mathbf{n}\cdot\boldsymbol{\sigma}/\omega^2} e^{-i m^* a_c(t) x \mathbf{n}\cdot\boldsymbol{\sigma}}, \tag{4}$$

$$\mathcal{X}_\xi = e^{im^*[x-x_c(t)]\dot{x}_c(t)} e^{-ix_c(t)p} I. \tag{5}$$

Here $\psi_m(x)$ represents the mth eigenstate of a harmonic oscillator with eigenenergy $\omega_m = (m+1/2)\omega$ and $|\chi_s\rangle$ is spinor of the electron in the eigenbasis of operator σ_z. The phase $\phi_\xi(t) = -\int_0^t L_\xi(t')\mathrm{d}t'$ is the coordinate action integral, where $L_\xi(t) = m^*\dot{x}_c^2(t)/2 - m^*\omega^2[x_c(t)-\xi(t)]^2/2$ is the Lagrange function of a driven harmonic oscillator and $x_c(t)$ is the solution to the equation of motion of a classical driven oscillator

$$\ddot{x}_c(t) + \omega^2 x_c(t) = \omega^2 \xi(t). \tag{6}$$

Another phase factor is the SOI action integral phase $\phi_\alpha(t) = -\int_0^t L_\alpha(t')\mathrm{d}t'$, with $L_\alpha(t) = m^*\dot{a}_c^2(t)/(2\omega^2) - m^*[a_c(t)-\alpha(t)]^2/2 + m^*\alpha^2(t)/2$ being the Lagrange function of another driven oscillator, satisfying $\ddot{a}_c(t) + \omega^2 a_c(t) = \omega^2\alpha(t)$.

In this paper, we consider particularly interesting cyclic transformations with periodic drivings $\xi(T) = \xi(0)$ and $\alpha(T) = \alpha(0)$ with zero values and time derivatives of responses x_c and a_c at times $t = 0$ and $t = T$. The spin-qubit is for such drivings rotated around $\mathbf{n}$ by the angle $\phi = -2m^*\int_0^T \dot{a}_c(t')\xi(t')\mathrm{d}t'$.[21]

We assume noise in the driving function $\xi(t) = \xi^0(t) + \delta\xi(t)$ consisting of ideal driving part without noise $\xi^0(t)$ with superimposed stochastic part with vanishing mean $\langle\delta\xi(t)\rangle = 0$. We consider the Ornstein–Uhlenbeck colored noise[42,43] characterized by the autocorrelation function $\langle\delta\xi(t')\delta\xi(t'')\rangle = \frac{\sigma_\xi^2}{2\tau_\xi} e^{|t'-t''|/\tau_\xi}$, with noise intensity σ_ξ^2 and correlation time τ_ξ. A general solution of equation (6) $x_c(t)$ with $x_c(0) = \xi^0(0)$ and $\dot{x}_c(0) = 0$ is given by

$$x_c(t) = \xi^0(0) + \omega\int_0^t \sin[\omega(t-t')]\xi(t')\mathrm{d}t', \tag{7}$$

which due to the noise term $\delta\xi$ is normally distributed with the variance evaluated as equal-times autocorrelation function,

$$\sigma_x^2(t) = \omega^2 \lim_{\Delta t\to 0}\left\langle \int_0^t \sin[\omega(t-t')]\delta\xi(t')\mathrm{d}t' \int_0^{t+\Delta t} \sin[\omega(t-t'')]\delta\xi(t'')\mathrm{d}t''\right\rangle. \tag{8}$$

For the Ornstein–Uhlenbeck noise considered here, the integrals can be evaluated exactly. Nevertheless, here we consider only the white noise limit where $\tau_\xi \to 0$ and $\langle\delta\xi(t')\delta\xi(t'')\rangle = \sigma_\xi^2\delta(t'-t'')$ leading to the variances

$$\sigma_x^2(t) = \frac{1}{4}\omega\sigma_\xi^2(2\omega t - \sin 2\omega t) \quad \text{and} \quad \sigma_{\dot{x}}^2(t) = \frac{1}{4}\omega^3\sigma_\xi^2[2\omega t + \sin(2\omega t)], \tag{9}$$

corresponding to $x_c(t)$ and $\dot{x}_c(t)$, respectively.

In addition to the noise in the potential minimum position $\xi(t)$, we consider also noise in SOI driving function $\alpha(t) = \alpha^0(t) + \delta\alpha(t)$, where $\alpha^0(t)$ is ideal noiseless driving. SOI noise $\delta\alpha(t)$ is similar to the previous case of spatial driving and is again of the Ornstein–Uhlenbeck type of autocorrelation function $\langle\delta\alpha(t')\delta\alpha(t'')\rangle$ with noise intensity σ_α^2 and correlation time in the white noise limit $\tau_\alpha \to 0$, leading to the time-dependent variances $\sigma_a^2(t) = (\sigma_\alpha/\sigma_\xi)^2\sigma_x^2(t)$ and $\sigma_{\dot{a}}^2(t) = (\sigma_\alpha/\sigma_\xi)^2\sigma_{\dot{x}}^2(t)$ for $a_c(t)$ and $\dot{a}_c(t)$, respectively.

3. Fidelity of Noisy Qubit Transformations

As an example of effects of noise to spin-qubit transformations, we consider driving corresponding to the class of circular paths in two-dimensional coordinate-SOI space $\mathcal{C}_{\rm ad} \sim \alpha^0[\xi]$,

$$\xi^0(t) = \xi_0 \cos(\omega t/n) \quad \text{and} \quad \alpha^0(t) = \alpha_0 \sin(\omega t/n), \tag{10}$$

where $n \geq 2$ is integer, and the period of the transformation is $T = 2\pi n/\omega$. Periodic responses represent contours $\mathcal{C} \sim a_c^0[\xi]$, where

$$a_c^0(t) = \alpha_0 \frac{n[n\sin(\omega t/n) - \sin(\omega t)]}{n^2 - 1}, \tag{11}$$

with the phases given by the area in the coordinate-SOI plane,

$$\phi_{\rm ad} = -2m^* \int_0^T \dot{\alpha}^0(t')\xi(t')\mathrm{d}t' = -2m^* \oint_{\mathcal{C}_{\rm ad}} \alpha^0[\xi]\mathrm{d}\xi = -2\pi m^* \xi_0 \alpha_0, \tag{12}$$

$$\phi^0 = -2m^* \oint_{\mathcal{C}} a_c^0[\xi]\mathrm{d}\xi = \frac{n^2}{n^2-1}\phi_{\rm ad}. \tag{13}$$

The adiabatic angle $\phi_{\rm ad}$ corresponds to the one when circular driving is of type $n \to \infty$. Transformation angle $\phi = \phi^0 + \delta\phi$ is due to the noise distributed normally around the mean ϕ^0, with the variance after one cycle given by[41]

$$\frac{\sigma^2_{\phi,n}}{\phi^2_{\rm ad}} = \frac{n(1+n^2)}{\pi(n^2-1)^2}\frac{\omega\sigma_\xi^2}{\xi_0^2} + \frac{2n^3}{\pi(n^2-1)^2}\frac{\omega\sigma_\alpha^2}{\alpha_0^2} + n^2\left(\frac{\omega\sigma_\xi\sigma_\alpha}{\xi_0\alpha_0}\right)^2. \tag{14}$$

Figure 1(a) shows spin–orbit responses as a function of time and Fig. 1(b) shows the contour $\mathcal{C}$ for the case of circular driving equation (10) with $n = 6$. In both panels, the dashed black lines denote noiseless spin–orbit driving $\alpha^0(t)$ and the red line denotes noiseless spin–orbit response $a_c^0(t)$. The focus is on the set of 10 spin–orbit responses $a_c(t)$ to 10 different realizations of white noise in

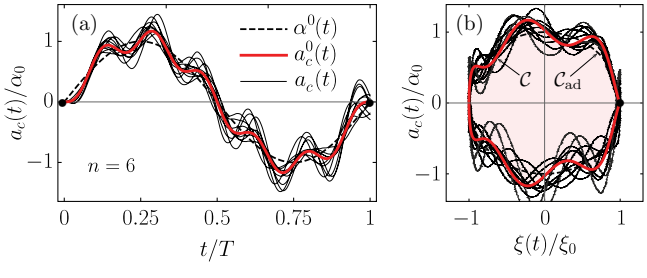

Fig. 1. (Color online) Responses to circular driving with $n = 6$ are shown. In (a) are as functions of time shown noiseless driving $\alpha^0(t)$ (dashed line), noiseless response $a_c^0(t)$ (red) and 10 responses $a_c(t)$ (black lines) to different realizations of white noise $\delta\alpha(t)$ with intensity $\sigma_\alpha = \alpha_0/(20\sqrt{\omega})$. Bullets denote noiseless starting $[a_c^0(0), \xi^0(0)]$ and ending positions $[a_c^0(T), \xi^0(T)]$. In (b) are shown the same quantities as in (a) but as a function of coordinate driving $\xi(t)$ with $\sigma_\xi = \xi_0/(20\sqrt{\omega})$. The noiseless contours $\alpha^0[\xi]$ and $a_c^0[\xi]$ form closed loops, $\mathcal{C}_{\rm ad}$ and $\mathcal{C}$, respectively. Note that ϕ is proportional to pink shaded area enclosed by $\mathcal{C}$.

$\alpha(t)$. $\sigma_a^2(t)$ manifests as a spread of these curves around the ideal noiseless red line. Bullets correspond to initial $[a_c^0(0), \xi^0(0)]$ and final noiseless values $[a_c^0(T), \xi^0(T)]$ of noiseless response and show that the final values of $a_c(T)$ deviate from the desired ones. The noisy response is not periodic, resulting in open loop in parameter space unlike the case of noiseless $\mathcal{C}$ and noiseless adiabatic driving $\mathcal{C}_{\rm ad}$. Consequently, the angle of spin rotation cannot be expressed as an area enclosed by the contour as in Eq. (13) and in Fig. 1(b) (pink shaded). It should be noted that, in general, the total angle of spin rotation ϕ is less prone to noise because the noisy curves oscillate around the ideal value and so contributions to final error partially cancel out.[41]

This analysis of spin-rotation angle demonstrated that due to gate noise in the driving functions, spin transformations are not completely faithful. For nonadiabatic qubit manipulations, the electron state is determined by the time-dependent Hamiltonian during the evolution and is, in general, a superposition of excited states, ultimately becoming the ground state when the transformation is complete. Therefore, in addition to correct transformation of the spin direction, one has also to take care that the electron state has not left the starting energy manifold at the final time. As shown in Refs. 20, 21 and 30 such motions in parametric space can easily be performed if the driving functions are appropriately chosen. Here, an important question is relevant: how well does the final state of the electron relax to the desired final state energy manifold after the transformation if the driving function is not ideal as in the presence of noise?

In order to demonstrate how to answer this question, in general, we consider the qubit wave function $|\Psi_{0\frac{1}{2}}(t)\rangle$, Eq. (2), which is at $t = 0$ in the ground state of the harmonic quantum dot (with $m = 0$) and spin $\frac{1}{2}$. We observe its relaxation to the ground state manifold that is spanned by two basis states[20] of time-dependent Hamiltonian equation (1) at time t,

$$|\widetilde{\Psi}_{0s}\rangle = e^{-im^*[x-\xi(t)]\alpha(t)\mathbf{n}\cdot\boldsymbol{\sigma}}|\psi_0[x-\xi(t)]\rangle|\chi_s\rangle. \tag{15}$$

As the appropriate measure of the relaxation accuracy, we define fidelity $F = \langle\Psi_{0\frac{1}{2}}(t)|P_0|\Psi_{0\frac{1}{2}}(t)\rangle$, where $P_0 = \sum_s |\widetilde{\Psi}_{0s}\rangle\langle\widetilde{\Psi}_{0s}|$ is the projector onto the ground state manifold. We choose $\mathbf{n}$ perpendicular to the z-axis and a straightforward derivation leads to the expression for overlaps of $|\Psi_{0\frac{1}{2}}(t)\rangle$ with the basis states at time t,

$$\langle\widetilde{\Psi}_{0\pm\frac{1}{2}}(t)|\Psi_{0\frac{1}{2}}(t)\rangle = \frac{1}{2}[e^{-\frac{1}{2}E_+(t)} \pm e^{-\frac{1}{2}E_-(t)}], \tag{16}$$

where

$$E_\pm(t) = \frac{m^*}{2\omega}\{[\omega(x_c(t)-\xi(t)) \pm \dot{a}_c(t)/\omega]^2 + [\dot{x}_c(t) \mp (a_c(t)-\alpha(t))]^2\} \tag{17}$$

resembles classical energy with additional terms for spin–orbit coupling and is equal to the classical energy if the spin–orbit driving is constant.[20] Ideal qubit transformations with spin-fidelities $\mathcal{F}_s = |\langle\widetilde{\Psi}_{0s}|\Psi_{0\frac{1}{2}}\rangle|^2 = \delta_{s\frac{1}{2}}$ are achieved by applying ideal drivings, where the energies $E_\pm$ vanish at final time $t = T$, i.e., when $x_c = \xi$, $a_c = \alpha$, $\dot{x}_c = 0$ and $\dot{a}_c = 0$.

The fidelity at arbitrary time t is obtained by summation over final spin states,

$$F(t) = \sum_s \mathcal{F}_s(t) = \frac{1}{2}[e^{-E_+(t)} + e^{-E_-(t)}]. \tag{18}$$

The presence of noise in spin–orbit and spatial driving terms makes fidelity a random quantity, $F(t) = F^0(t) + \delta F(t)$, where $F^0(t)$ represents the result of noiseless driving and $\delta F(t)$ is the deviation from this value. Fidelity is therefore characterized by some probability density function $\frac{\mathrm{d}P(F)}{\mathrm{d}F}$. It can be calculated from the probability density for variables $E_\pm$ which are functions of independent random variables and normally distributed. The probability density functions for $E_\pm$ at time t can be calculated using the formula

$$\left.\frac{\mathrm{d}P_\pm(E)}{\mathrm{d}E}\right|_t = \iiiint \delta[E - E_\pm(x_c, \dot{x}_c, a_c, \dot{a}_c)] \times \frac{\mathrm{d}P_x(x_c)}{\mathrm{d}x_c}\frac{\mathrm{d}P_{\dot{x}}(\dot{x}_c)}{\mathrm{d}\dot{x}_c}\frac{\mathrm{d}P_a(a_c)}{\mathrm{d}a_c}\frac{\mathrm{d}P_{\dot{a}}(\dot{a}_c)}{\mathrm{d}\dot{a}_c}\mathrm{d}x_c\mathrm{d}\dot{x}_c\mathrm{d}a_c\mathrm{d}\dot{a}_c. \tag{19}$$

The result is obtained by first calculating the characteristic functions,

$$p_\pm(k) = \int_{-\infty}^{\infty} \frac{\mathrm{d}P_\pm(E)}{\mathrm{d}E} e^{ikE}\mathrm{d}E = \frac{2\sigma_1^{-1}\sigma_2^{-1}}{\sqrt{(2\sigma_1^{-2} - ik)(2\sigma_2^{-2} - ik)}}, \tag{20}$$

with

$$\sigma_1^2(t) = \left(\frac{2m^*}{\omega}\right)[\omega^2\sigma_x^2(t) + \sigma_{\dot{a}}^2(t)/\omega^2], \tag{21}$$

$$\sigma_2^2(t) = \left(\frac{2m^*}{\omega}\right)[\sigma_{\dot{x}}^2(t) + \sigma_a^2(t)]. \tag{22}$$

Note the equality $p_+(k) = p_-(k)$ which after the inverse Fourier transform yields equal functional forms for E_+ and E_-,

$$\left.\frac{\mathrm{d}P_\pm(E_\pm)}{\mathrm{d}E_\pm}\right|_t = 2\sigma_1^{-1}\sigma_2^{-1} I_0[(\sigma_1^{-2} - \sigma_2^{-2})E_\pm]e^{-(\sigma_1^{-2}+\sigma_2^{-2})E_\pm}, \tag{23}$$

where $I_0(z)$ is the modified Bessel function of the first kind.

Since the fidelity is a sum of two dependent random variables, its probability distribution is calculated from the joint probability distribution function for those two variables, which in general cannot be evaluated analytically. However, one can examine $\frac{\mathrm{d}P}{\mathrm{d}F}$ exactly when $\sigma_x^2(t) = \sigma_{\dot{a}}^2(t)/\omega^4$ and $\sigma_{\dot{x}}^2(t) = \sigma_a^2(t)$, which is satisfied for $t = T$ if the coordinate and the SOI driving noise intensities are equal, i.e., $\sigma_\alpha = \omega\sigma_\xi$. In this case, E_+ and E_- become *independent* random variables and $\frac{\mathrm{d}P}{\mathrm{d}F}$ can be calculated as the convolution of probability distributions for e^{-E_+} and e^{-E_-}. At $t = T$, the exact result for $F \geq \frac{1}{2}$ is given by

$$\left.\frac{\mathrm{d}P(F)}{\mathrm{d}F}\right|_{t=T} = 2\sigma_F^{-4}\left[B\left(\frac{1}{2F}, \sigma_F^{-2}, \sigma_F^{-2}\right) - B\left(1 - \frac{1}{2F}, \sigma_F^{-2}, \sigma_F^{-2}\right)\right](2F)^{2\sigma_F^{-2}-1}, \tag{24}$$

where $B(x,a,b)$ is the incomplete beta function and $\sigma_F^{-2} = \sigma_1^{-2} + \sigma_2^{-2}$. For $F < \frac{1}{2}$, the probability distribution is $\frac{dP}{dF} = 2\sigma_F^{-4} B(\sigma_F^{-2}, \sigma_F^{-2})(2F)^{2\sigma_F^{-2}-1}$, where $B(a,b)$ is the beta function. In practice, where noise intensities are small, the most relevant regime is $\sigma_F \to 0$ for which the probability distribution equation (24) simplifies to $\frac{dP}{dF} \propto (1-F)F^{2\sigma_F^{-2}}$. Due to similar dependence of $\mathcal{F}_s$ and F on $E_\pm$, it is easy to derive analytical results also for spin-fidelity probability distributions $\frac{dP_s}{d\mathcal{F}_s}$ (not shown here).

In Fig. 2(a), different realizations of noisy fidelity (black lines) are compared to the noiseless one (red) for $n = 2$. One can observe that noisy fidelity starts to deviate from the noiseless one for $t/T \gtrsim 0.1$, reaches maximum deviation at $t/T \sim 0.5$ and then deviations are again lowered when approaching $t \to T$. The same quantities are presented in Fig. 2(c) for circular driving with $n = 8$ where the noiseless curve is denoted with blue color. Figure 2(b) shows noiseless curves $a_c[\xi]$ in parametric space during the transformation with $n = 2$ (red), $n = 8$ (blue, dashed) and $n \to \infty$ (black, dashed), the latter corresponding to the adiabatic limit. Bullets denote initial and final values of $a_c(t)$ and $\xi(t)$. Note that the motion is periodic

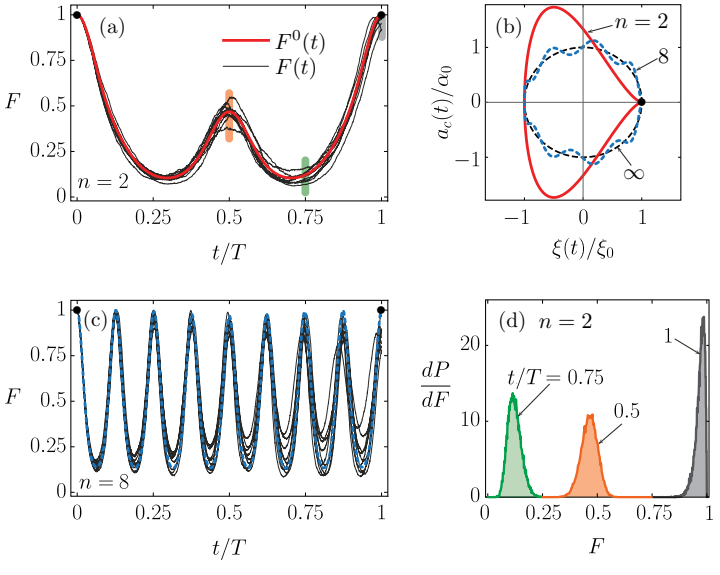

Fig. 2. (Color online) In panel (a) the noiseless fidelity $F^0(t)$ (red line) and 10 fidelities $F(t)$ (black lines) for different realizations of white noise with intensities $\sigma_\xi/\xi_0 = \sigma_\alpha/\alpha_0 = 1/(20\sqrt{\omega})$ are shown as functions of time when driving the system circularly with $n = 2$. Orange, gray and green shaded regions at times $t/T = 0.5, 0.75, 1$, correspondingly, show the spread of noisy fidelities around the exact value. Noiseless contours in parameter space $[a_c, \xi]$ are for $n = 2$ (red), 8 (blue, dashed) and $n \to \infty$ (black, dashed) presented in panel (b). Panel (c) shows the same as panel (a) for circular driving with $n = 8$ and the noiseless fidelity is denoted with blue line. Bullets mark initial and final values of noiseless fidelity in (a) and (c) and contour in parameter space in (b). In panel (d) probability density distributions of fidelity for $n = 2$ at times $t/T = 0.5$ (orange), $t/T = 0.75$ (green) and $t = T$ (gray) are shown. Color codes coincide with the area of fidelity spreading shown in (a). Distributions were generated from $N = 10^7$ samples.

with period T and that $a_c(0) = a_c(T) = \alpha(0) = \alpha(T)$ as is manifested also in noiseless fidelity being equal to 1 at $t = 0$ and $t = T$, as a demonstration that the system returns to the ground state manifold with probability 1. This can be seen from positions of bullets in Figs. 2(a) and 2(c). Figure 2(d) shows the probability density distribution of fidelity at times $t/T = 0.5$ (orange), $t/T = 0.75$ (green) and $t = T$ (black). It should be mentioned that the distribution for $t = T$ is given also by the exact formula, Eq. (24). The color code of distributions corresponds to the code of the shading of fidelity spreading around the noiseless value in Fig. 2(a). Distributions are centered around noiseless values and their variances are proportional to spreadings observed in Fig. 2(a), the distribution at $t/T = 0.5$ having the largest variance which is lower at $t/T = 0.75$ and even lower at $t = T$.

4. Summary

We presented an analysis of spin-qubit nonadiabatic manipulation of an electron trapped in a moving linear harmonic trap and in the presence of time-dependent Rashba interaction. One of the main challenges here is a precise tuning of driving fields since the electron starting from the ground state should after performing one cycle with time-dependent Hamiltonian return to the ground state, although during the cycle the state of the electron is a superposition of excited eigenstates of the moving trap.

The problem is even more subtle because there will always be present some noise in driving functions, which means that spin-qubit transformation will always deviate from the ideal one. Since for the model considered here exact solutions are available for a broad class of drivings, we concentrated also to the exact analysis of the influence of small deviations from ideal qubit manipulation. In particular, we focused to an explicit example and demonstrated how one can analyze the effects of a general noise to the transformation angle and we showed the results for the Ornstein–Uhlenbeck type of noise.

An example, considered in detail, is the case of circular driving in the space of parameters for which exact analytical formulae are given and analyzed for white noise. In view of the fact that for nonadiabatic regimes a nontrivial point is the ability of the system to return to the ground state after an arbitrary time-dependent driving, our analysis was focused to the fidelity — the overlap of the actual wave function with the desired ideal. For white noise, explicit formulae are derived for symmetric noise intensities in position and spin–orbit driving functions. A detailed derivation and analysis of fidelity are presented. Additionally, analytical results are illustrated by special cases of driving together with numerically generated noisy drivings and the corresponding responses.

Acknowledgments

The authors acknowledge support from the Slovenian Research Agency under contract No. P1-0044.

References

1. S. A. Wolf *et al.*, *Science* **294**, 1488 (2001).
2. I. Žutić and S. Das Sarma, *Rev. Mod. Phys.* **76**, 323 (2004).
3. E. I. Rashba, *Future Trends in Microelectronics* (John Wiley & Sons, Hoboken, NJ, USA, 2007).
4. D. D. Awschalom *et al.*, *Science* **339**, 1174 (2013).
5. R. Winkler, *Two-Dimensional Electron and Hole Systems*, Springer Tracts in Modern Physics, Vol. 191 (Springer, Berlin, Heidelberg, 2003).
6. H.-A. Engel, E. I. Rashba and B. I. Halperin, *Handbook of Magnetism and Advanced Magnetic Materials* (John Wiley & Sons, Chichester, UK, 2007).
7. G. Dresselhaus, *Phys. Rev.* **100**, 580 (1955).
8. E. I. Rashba, *Sov. Phys. Solid State* **2**, 1109 (1960).
9. J. Nitta *et al.*, *Phys. Rev. Lett.* **78**, 1335 (1997).
10. T. Schapers *et al.*, *J. Appl. Phys.* **83**, 4324 (1998).
11. J. Nitta, F. E. Meijer and H. Takayanagi, *Appl. Phys. Lett.* **75**, 695 (1999).
12. J. Schliemann, J. C. Egues and D. Loss, *Phys. Rev. Lett.* **90**, 146801 (2003).
13. J. Wunderlich *et al.*, *Science* **330**, 1801 (2010).
14. A. Gómez-León and G. Platero, *Phys. Rev. B* **86**, 115318 (2012).
15. J. Pawlowski, P. Szumniak and S. Bednarek, *Phys. Rev. B* **93**, 045309 (2016).
16. J. Pawlowski, P. Szumniak and S. Bednarek, *Phys. Rev. B* **94**, 155407 (2016).
17. J. Fan *et al.*, *Sci. Rep.* **6**, 38851 (2016).
18. S. Kruchinin and H. Nagao, *Int. J. Mod. Phys. B* **26**, 1230013 (2012).
19. S. Kruchinin and T. Pruschke, *Phys. Lett. A* **378**, 157 (2014).
20. T. Čadež, J. H. Jefferson and A. Ramšak, *New J. Phys.* **15**, 013029 (2013).
21. T. Čadež, J. H. Jefferson and A. Ramšak, *Phys. Rev. Lett.* **112**, 150402 (2014).
22. M. Büttiker, Y. Imry and R. Landauer, *Phys. Lett. A* **96**, 365 (1983).
23. A. Fuhrer *et al.*, *Nature* **413**, 822 (2001).
24. A. Aronov and Y. Lyanda-Geller, *Phys. Rev. Lett.* **70**, 343 (1993).
25. T.-Z. Qian and Z.-B. Su, *Phys. Rev. Lett.* **72**, 2311 (1994).
26. A. Mal'shukov, V. Shlyapin and K. Chao, *Phys. Rev. B* **60**, R2161 (1999).
27. K. Richter, *Physics* **5**, 22 (2012).
28. F. Nagasawa *et al.*, *Nat. Commun.* **4**, 2526 (2013).
29. H. Saarikoski *et al.*, *Phys. Rev. B* **91**, 241406(R) (2015).
30. A. Kregar, J. H. Jefferson and A. Ramšak, *Phys. Rev. B* **93**, 075432 (2016).
31. A. Kregar and A. Ramšak, *Int. J. Mod. Phys. B* **30**, 1642016 (2016).
32. P. San-Jose *et al.*, *Phys. Rev. Lett.* **97**, 076803 (2006).
33. P. San-Jose *et al.*, *Phys. Rev. B* **77**, 045305 (2008).
34. P. Huang and X. Hu, *Phys. Rev. B* **88**, 075301 (2013).
35. C. Echeverría-Arrondo and E. Y. Sherman, *Phys. Rev. B* **87**, 081410(R) (2013).
36. J. Mravlje, A. Ramšak and T. Rejec, *Phys. Rev. B* **74**, 205320 (2006).
37. J. Mravlje and A. Ramšak, *Phys. Rev. B* **78**, 235416 (2008).
38. T. Rejec, A. Ramšak and J. H. Jefferson, *J. Phys. Condens. Matter* **12**, L233 (2000).
39. J. H. Jefferson, A. Ramšak and T. Rejec, *Europhys. Lett.* **74**, 764 (2006).
40. G. Giavaras *et al.*, *Phys. Rev. B* **74**, 195341 (2006).
41. L. Ulčakar and A. Ramšak, *New J. Phys.* **19**, 093015 (2017).
42. M. C. Wang and G. E. Uhlenbeck, *Rev. Mod. Phys.* **17**, 323 (1945).
43. J. Masoliver, *Phys. Rev. A* **45**, 706 (1992).
44. S. Nadj-Perge *et al.*, *Phys. Rev. Lett.* **108**, 166801 (2012).